Journal of Drug Delivery Science and Technology 55 (2020) 101371

Contents lists available at ScienceDirect

Journal of Drug Delivery Science and Technology

journal homepage: www.elsevier.com/locate/jddst

A wet-milling method for the preparation of cilnidipine nanosuspension with enhanced dissolution and oral bioavailability

Qiang Liu[a], Yaping Mai[a], Xiangshuai Gu[a], Yue Zhao[a], Xin Di[b], Xueqin Ma[b], Jianhong Yang[a,*]

[a] Department of Pharmaceutics, School of Pharmacy, Ningxia Medical University, No.1160 Shengli South Street, Yinchuan, 750004, PR China
[b] Department of Pharmaceutical Analysis, School of Pharmacy, Ningxia Medical University, No.1160 Shengli South Street, Yinchuan, 750004, PR China

ARTICLE INFO

Keywords:
Cilnidipine
Nanosuspension
Wet-milling
Bioavailability

ABSTRACT

Cilnidipine (CLD) is extensively used in the treatment of hypertension; however, it has extremely low solubility which limits its clinical application. The purpose of the present research was to improve the dissolution rate and oral bioavailability of CLD by preparing a nanosuspension. The CLD nanosuspension (CLD-NS) was developed using a wet-milling method with PVP VA64 as the steric stabilizer and SLS as the electrostatic stabilizer. The formulated CLD-NS displayed a narrow and uniform particle size distribution with a mean particle size of 312 nm, and a marked increase in the dissolution of CLD-NS in different dissolution media was observed compared with bulk CLD. The crystallinity of the drug and molecular interactions between drug and stabilizers were investigated by differential scanning calorimetry (DSC), X-ray powder diffraction (PXRD), Fourier transform infrared spectroscopy (FT-IR), and Raman spectroscopy, respectively. Furthermore, the *in vivo* pharmacokinetics of the formulated CLD-NS were evaluated in Sprague-Dawley rats by high-performance liquid chromatography coupled with tandem mass spectrometry (HPLC-MS/MS). The results indicated that the C_{max} and $AUC_{0\text{-}24}$ of CLD-NS were 3.13-fold and 2.38-fold higher than those of bulk CLD, respectively. Moreover, the C_{max} and $AUC_{0\text{-}24}$ of CLD-NS were increased 1.65-fold and 2.17-fold, compared with commercial CLD capsules. These results indicated the significant increase in CLD bioavailability.

1. Introduction

Cilnidipine (CLD) is a novel dihydropyridine Ca^{2+} antagonist which can effectively inhibit both L-type Ca^{2+} channels on vascular smooth muscle and N-type Ca^{2+} channels on sympathetic neurons, and is successfully used in the clinical treatment of hypertension. Available studies indicate that CLD (pKa = 11.39, ClogP = 5.54) belongs to class II of the Biopharmaceutics Classification System (BCS) [1] and has very low crystalline solubility (0.03–0.06 μg/mL) and amorphous solubility (0.3–2.3 μg/mL) in buffer or other biologically relevant media at different pH values [2–4]. Such extremely low solubility in aqueous media results in a low dissolution velocity and oral bioavailability of the solid formulation and further limits its clinical therapeutic effect. Thus, over the past decades, formulation scientists have tried different technological strategies to overcome this drawback, including microemulsion [1], solid dispersion [5], a cyclodextrin inclusion complex [6], a solid self-emulsifying drug delivery system (solid-SEDDS) [7], and a nanosuspension [8]. However, most of these studies were focused on investigating the enhancement of solubility and *in vitro* dissolution, and few studies evaluated the *in vivo* bioavailability of CLD based on formulation technology. In addition, despite some exploratory studies, the availability of industrial production is unclear.

In recent years, nanosuspension has been successfully used to improve the solubility, dissolution rate and bioavailability of poorly water-soluble drugs, and include curcumin nanosuspensions [9], celecoxib nanosuspensions [10], efonidipine hydrochloride nanosuspensions [11], and lacidipine nanocrystals [12]. Nanosuspensions exhibit unique advantages, such as high drug loading, low toxicity and side effects, and improved safety [13]. Techniques for manufacturing nanosuspensions are divided into top-down and bottom-up methods [14]. Wet-milling, an effective top-down method, is regarded as the most promising technique of the many already developed preparation methods, due to its organic solvent-free technique and easy scale-up in industrial production. Several drug nanosuspensions based on wet-milling technology have been marketed over the past decades [15–17]. However, the instability of nanosuspensions is a problem as a nanosuspension is a thermodynamically unstable system [18,19]. Thus, stabilizers are essential excipients in nanosuspensions and the selection of suitable stabilizers is vital in the preparation of nanosuspensions [20,21]. Stabilization is mainly attained by steric hindrance provided

* Corresponding author. School of Pharmacy, Ningxia Medical University, No.1160 Shengli South Street, Yinchuan, 750004, PR China. Tel.: +8618809589768.
E-mail address: pharmacyy217@163.com (J. Yang).

https://doi.org/10.1016/j.jddst.2019.101371
Received 27 August 2019; Received in revised form 17 October 2019; Accepted 4 November 2019
Available online 05 November 2019
1773-2247/

by polymers and nonionic surfactants, and electrostatic repulsion provided by charged surfactants and polymers as well as the combination of steric and electrostatic effects [13,22–24].

The combination of hydrophilic polymers and surfactants (especially SLS) was confirmed to significantly improve the stability of nanosuspensions in previous research [25]. These polymers include hydroxypropyl cellulose (HPC), hydroxypropyl methyl cellulose (HPMC), polyvinylpyrrolidone (PVP), polyvinyl alcohol (PVA), Poloxamers, and Soluplus®. Kollidon® VA64 (PVP VA64), is a vinyl pyrrolidone-vinyl acetate water soluble copolymer and consists of long polymer chains with hydrophilic and hydrophobic groups [26]. It was reported that PVP VA64 can adsorb on the surface of the drug particle and resist particle aggregation [27]. In the present study, PVP VA64 and SLS were chosen as steric and electrostatic stabilizers to fabricate CLD-NS using the wet-milling method. The physicochemical properties of the obtained CLD-NS such as particle size, polydispersity index (PDI), zeta potential, morphology, and crystalline state were systematically characterized. Furthermore, the stability and *in vitro* dissolution performance of CLD-NS were investigated. Finally, the *in vivo* pharmacokinetics in Sprague-Dawley (SD) rats were evaluated by HPLC-MS/MS, in comparison with CLD powder and commercial capsules.

2. Materials and methods

2.1. Materials

CLD (purity > 98%) was kindly donated by NingXia DuoWei Pharmaceutical Co., Ltd. (Yinchuan, China). Nimodipine, used as the reference substance, was purchased from the National Institutes for Food and Drug Control (Beijing, China). Kolliphor® SLS fine was provided by Beijing Fengli Jingqiu Pharmaceutical Co., Ltd. (Beijing, China). Kollidon® VA64 (PVP VA64) was supplied by BASF Corporation (Ludwigshafen, Germany). Carboxymethylcellulose sodium (CMC-Na) was obtained from Anhui Sunhere Pharmaceutical Excipients Co., Ltd. (Huainan, China). Acetonitrile (HPLC grade), methanol (HPLC grade) and ammonium acetate (HPLC grade, ≥99.0%) were purchased from Thermo Fisher Scientific Inc. (Beijing, China) and Shanghai Macklin Biochemical Co., Ltd. (Shanghai, China), respectively.

2.2. Preparation of CLD nanosuspension

In our previous experiments, we selected several types of stabilizers (HPMC-E5, PVP K30, poloxamer 188, poloxamer 407, TPGS, PEG6000, HPC-SSL, and SLS) to fabricate CLD-NS and found that the above dispersants did not stabilize CLD-NS. In addition, we screened the effects of grinding time, grinding speed, and stabilizer concentration on the particle size and PDI of the nanosuspension (data not shown) and finally determined the formulation in the present study. Briefly, 0.3 g PVP VA64 and 0.05 g SLS were dissolved in 50 mL deionized water under magnetic stirring (JKI, Shanghai Jingxue Science Apparatus Co., Ltd, Shanghai, China), and the pH value of the stabilizer solution was 5.20 (25 °C). Then, 1g CLD powder was dispersed in the above solution and stirred for 10 min. The mixture was then placed in a Superfine Grinding Equipment (Mini-easy-MEM 015, Retsch Topway Technology Co., Ltd, Beijing, China) with zirconium oxide milling beads (0.6–0.8 mm diameter) as milling media. The milling chamber volume was approximately 150 mL and the volume of milling media was 140 mL, which occupied 93% of the milling chamber volume. The milling procedure was performed under circulating water cooling and the following parameters: milling rotation speed, 2,500 rpm; external stirrer rate, 260 rpm; and milling duration, 45 min.

2.3. Solidification of the CLD nanosuspension

In order to further improve the stability of the CLD nanosuspension and carry out late physicochemical characterization, the aqueous nanosuspension was freeze-dried using a FreeZone® 6 L freeze dryer (Labconco Corporation, Kansas City, MO, USA) to obtain the solid powder. Furthermore, the obtained solid CLD-NS powder was more advantageous for downstream processing of the CLD nanosuspension, such as further preparation into a solid dosage form to increase the stability of the nanosuspension and increase patient compliance. The lyophilization process was as follows: CLD nanosuspension was first poured into a stainless steel dish, sealed with a parafilm, prefrozen at −80 °C for 6 h and then quickly transferred to the lyophilizer and lyophilized at −50 °C and 12.5 pa for 24 h.

2.4. Characterization of the CLD nanosuspension

2.4.1. Particle size, zeta potential and redispersibility

CLD nanosuspension samples were diluted to approximately 1 mg/mL using deionized water and fully dispersed before testing. The particle size, PDI, and zeta potential of the CLD nanosuspension were measured using dynamic light scattering (Nano-ZS90, Malvern, Worcestershire, UK). All samples were examined in triplicate. The redispersibility of lyophilized CLD-NS powder was evaluated using the redispersibility index (RDI) [28]. In addition, the particle size, PDI and zeta potential of reconstitutable CLD-NS were also used to assess redispersibility.

2.4.2. Particle morphology

The morphology of bulk CLD and freeze-dried samples of CLD nanosuspension (CLD-NS powder) were examined by scanning electron microscopy (S-4800 SEM, Hitachi Ltd., Tokyo, Japan). Each sample was fixed onto the sample holder with double-sided sticky tape and sputtered with a thin layer of gold. The samples were then examined at an accelerating voltage of 5 kV.

2.4.3. Differential scanning calorimetry (DSC)

The thermograms of CLD, excipients (PVP VA64 and SLS), physical mixtures of CLD, PVP VA64 and SLS (CLD-PM), and CLD-NS powder were assessed using DSC (DSC 200F3 Maia®, Netzsch, Germany). Each sample was heated in an aluminum pan from 20 °C to 200 °C at a heating rate of 10 °C/min under a nitrogen gas atmosphere (70 mL/min). The enthalpy and temperature of the instrument were calibrated with indium before thermal analysis.

2.4.4. X-ray powder diffraction (PXRD)

The crystallinity and crystal structure variation of CLD, black excipients (PVP VA64 and SLS), physical mixtures, and CLD-NS powder were measured by a power X-ray diffractometer (X'pert pro X-ray diffractometer, PANalytical, Germany) with Cu Kα radiation (40 kV and 40 mA). The diffraction patterns of the samples were scanned from 3 to 50° (2θ) with a step size and scanning speed rate of 0.02° and 5°/min, respectively.

2.4.5. Fourier transform infrared spectroscopy (FT-IR)

The FT-IR spectra of CLD, excipients (PVP VA64 and SLS), physical mixtures, and CLD-NS powder were recorded in the range from 4000 to 400 cm^{-1} with a resolution of 1.0 cm^{-1} using an FT-IR spectrometer (Tensor 27, Bruker Optics, Germany).

2.4.6. Raman spectroscopy

Raman spectroscopy of CLD, black excipients (PVP VA64 and SLS), physical mixtures, and CLD-NS powder were obtained with Thermo Fisher DXR Raman Spectrometer (Thermo Fisher, USA). The operating conditions were as follows: shift change, 3200–200 cm^{-1}; exposure time, 10 s; scan, 1 time.

2.4.7. Physical stability study

The short-term physical stability of the prepared CLD nanosuspension was evaluated. The freshly prepared CLD nanosuspension was

stored at room temperature and at 4 °C for 4 weeks. The average particle size, PDI, and zeta potential were determined on the first day, and at 2 weeks and 4 weeks.

2.4.8. Saturation solubility and in vitro dissolution study

The saturation solubility of bulk CLD, physical mixtures and CLD-NS powder was determined in three different media. Briefly, excess amounts of each sample were added to 5 mL deionized water in sealed glass tubes and then the tubes were shaken for 72 h at 37.0 ± 0.5 °C and 100 rpm and shielded from light in a shaking water bath (THZ-100, Shanghai BluePard Instruments Co., Ltd, Shanghai, China). Samples were centrifuged at 4,000 rpm for 10 min and the supernatant was filtered through a 0.45 μm syringe filter. The residual filtrate was subsequently diluted to a suitable concentration and determined by UV-VIS spectrophotometry (UV-1780, Shimadzu Instruments (Suzhou) Co., Ltd. Suzhou, China) at 242 nm. All samples were measured in triplicate.

According to the dissolution method of CLD tablets in the Chinese Pharmacopoeia and the Japanese Orange Book, dissolution of CLD powder, physical mixtures, and CLD-NS powder were carried out in a dissolution tester (RC12AD, Tianjin Tianda Tianfa Technology Co., Ltd, China) using the paddle method. The experiments were performed at 37.0 ± 0.5 °C with a paddle speed of 75 rpm. Samples containing an amount equivalent to 5 mg CLD were added to 900 mL dissolution media (containing 0.1% Tween 80, w/v), hydrochloric acid solution (pH 1.2), distilled water and phosphate buffer (pH 6.8). 5 mL samples were collected at 5, 10, 15, 20, 30, 45 and 60 min and the same volume of fresh dissolution medium at the same temperature was immediately added. The samples were then filtered through a 0.45 μm syringe filter, the initial 1 mL was discarded and the residual filtrate was subsequently determined by UV-VIS spectrophotometry (UV-1780, Shimadzu Instruments (Suzhou) Co., Ltd., Suzhou, China) at 242 nm. The similarity factor (f_2) was calculated using the following equation to compare the dissolution behavior of different CLD formulas. When the f_2 value was < 50, the dissolution profiles were considered different, and an f_2 value between 50 and 100 suggested that the two dissolution curves compared were similar.

$$f_2 = 50 \times \log\left\{\left[1 + \frac{1}{n}\sum_{t=1}^{n}(R_t - T_t)^2\right]^{-0.5} \times 100\right\}$$

where n, R_t and T_t are the number of dissolution points, dissolution values for the reference and test batch at time point t, respectively.

2.5. In vivo pharmacokinetics

2.5.1. Animal experiments

Male SD rats (weighing 200 ± 20 g) were obtained from the Experimental Animal Center of Ningxia Medical University (Yinchuan, China). All animal studies were performed according to the Guidelines for the Care and Use of Laboratory Animals and were approved by the Committee of Ethics of Animal Experimentation of Ningxia Medical University. The rats were randomly distributed into three groups (n = 6). These animals were transferred to the laboratory for 7 days to acclimate to their new environment prior to the experiments and were fed a standard diet and water ad libitum. All groups were fasted for 12 h with free access to water prior to experimentation. The following morning, the *in vivo* pharmacokinetics of CLD powder (4 mg CLD powder dispersed in 20 mL 0.5% CMC-Na suspension), CLD capsule (one capsule dispersed in 25 mL deionized water) and CLD-NS (0.2 mg/mL, diluted with deionized water), which were administrated orally at a dose of 2.0 mg/kg of equivalent CLD powder, were determined. All samples were vortexed for 10 min to ensure total dispersion before oral administration. Blood samples (approximately 0.5 mL) were taken from the suborbital vein at predetermined times (5 min, 15 min, 30 min, 45 min, 1.0 h, 2.0 h, 3.0 h, 4.0 h, 6.0 h, 8.0 h, 12.0 h, and 24 h) after administration. The blood samples were subsequently transferred into Eppendorf tubes containing 20 μL heparin and were immediately centrifuged at 8,000 rpm for 10 min at room temperature. The obtained plasma was stored −80 °C until analysis.

2.5.2. Bioanalytical method

CLD in the plasma sample was determined using the deproteinization method. Ten μL internal standard solution (200 ng/mL nimodipine dissolved in methanol) and 500 μL acetonitrile were added to each of 100 μL of thawed plasma to precipitate the protein. The mixtures were stirred for 5 min and then centrifuged at 14,000 rpm for 10 min. The obtained supernatant (5 μL) was then injected into the HPLC-MS/MS system for analysis.

The HPLC-MS/MS system consisted of a TSQ QUANTUM ACCESS MAX Triple Quadrupole mass spectrometer equipped with an electrospray ionization (ESI) source (Thermo Fisher, USA) and an Agilent Eclipse Plus C18 column (2.1 × 50 mm, 1.8 μm, Agilent, USA). The mobile phase consisted of 70% acetonitrile and 30% ammonium acetate solution (5 mM) and the flow rate was 0.3 mL per min. Ionization was performed in the negative mode and MS/MS was operated at unit resolution in MRM mode. Transition ions *m/z* 491.5 → 356.8 and *m/z* 417.4 → 121.9 were selected for CLD and nimodipine, respectively.

The pharmacokinetic parameters of each formulation including the maximum plasma drug concentration (C_{max}), the time (T_{max}) to reach C_{max}, the area under the concentration-time curve (AUC_{0-24}) and terminal half-life ($t_{1/2}$) were calculated using DAS 2.0 software (Chinese Pharmacological Society, Beijing, China) [10].

2.6. Statistical analysis

All obtained results were expressed as mean ± SD values. Statistical significance was assessed by the *t*-test and ANOVA using SPSS 17.0 software. The results with a *p*-value less than 0.05 ($p \leq 0.05$) were considered statistically significant.

3. Results and discussion

3.1. Particle size, zeta potential, redispersibility and morphology

In this study, the final composition of the nanosuspension included 0.3 g PVP VA64 and 0.05 g SLS dissolved in 50 mL deionized water followed by 1 g CLD dispersed in the solution. The mean particle size of CLD-NS was 312.15 ± 7.19 nm. The PDI value of CLD-NS was 0.11 ± 0.01, which indicated good uniformity of the particles [29]. It was reported that an absolute zeta potential value more than 20 mV was sufficient to stabilize the nanosuspension [21,30–32]. The zeta potential value of the prepared CLD-NS was −33.63 ± 0.87 mV, which provided a guarantee for the theoretical stability of the CLD-NS. The particle size, PDI, zeta potential, and RDI of reconstitutable CLD-NS were 337.1 ± 5.44 nm, 0.16 ± 0.05, −31.17 ± 0.64 mV, and 108%, respectively. These results demonstrated that the lyophilized CLD-NS powder was well dispersed in water [28].

Fig. 1a and b shows the surface morphology of bulk CLD and CLD-NS, respectively. Bulk CLD (Fig. 1a) displayed a long-needle shape with a very large particle size, while CLD-NS (Fig. 1b) showed a continuous and irregular flaky shape of different sizes.

Kolliphor® SLS, an anionic surfactant, has a critical micelle concentration (CMC) in water of 8.2 mM (0.24% w/w) at ambient temperature [33]. Previous studies indicated that the concentration of SLS in nanosuspensions should be lower than the CMC to avoid particle growth via Oswald ripening [30]. The concentration of SLS was 3.4 mM (0.1% w/w) in this study, which is below the CMC of SLS.

3.2. DSC

DSC was performed to investigate the crystalline state and polymorphic nature of CLD in the nanosuspension. The DSC thermograms of

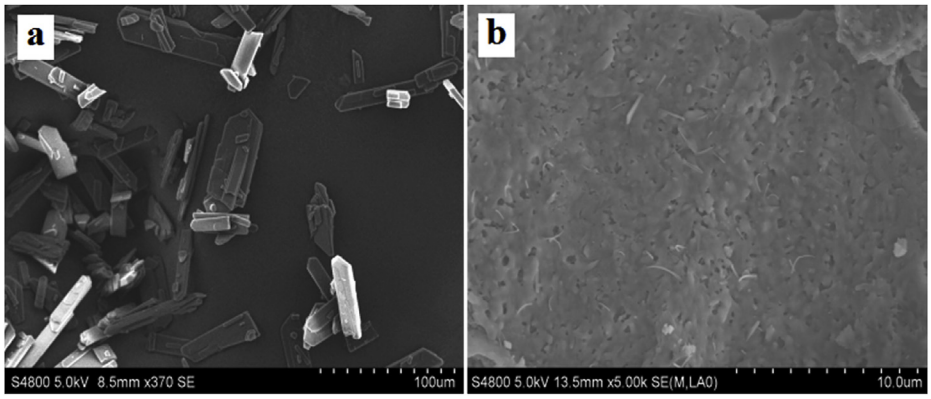

Fig. 1. SEM images of bulk CLD (a) and CLD-NS powder (b).

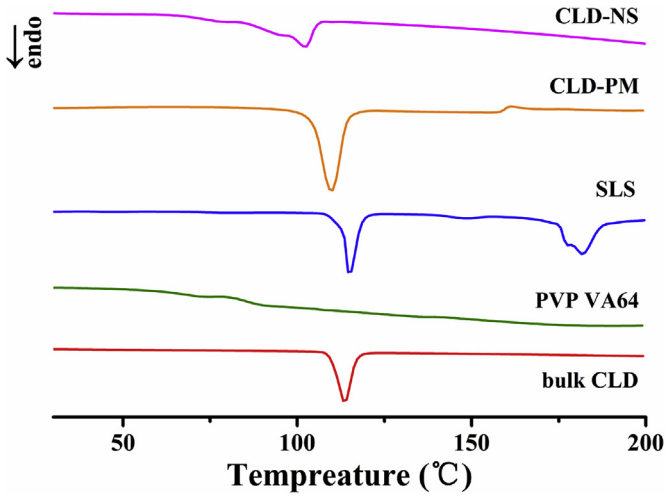

Fig. 2. DSC images for CLD powder, PVP VA64, SLS, physical mixtures of CLD, PVP VA64 and SLS and CLD-NS powder.

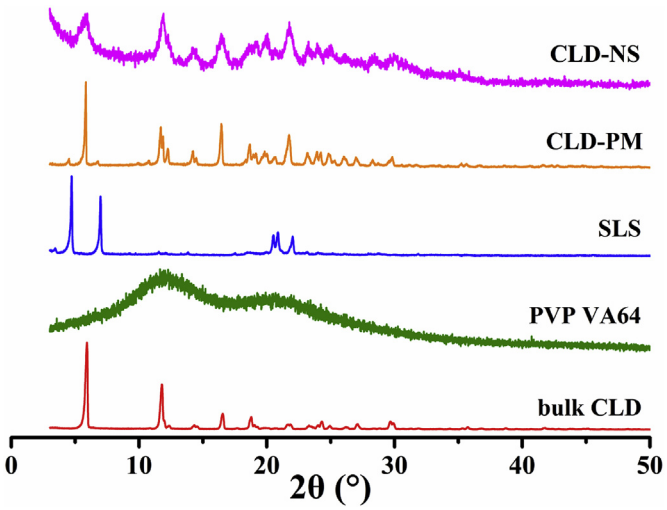

Fig. 3. PXRD patterns of CLD powder, PVP VA64, SLS, physical mixtures of CLD, PVP VA64 and SLS and CLD-NS powder.

bulk CLD, PVP VA64, SLS, physical mixtures, and CLD-NS are illustrated in Fig. 2. Bulk CLD showed a characteristic endothermic melting peak at 113.5 °C, while CLD-PM (109.7 °C) was similar to the melting peak of bulk CLD, but had a lower melting temperature, which could be due to the presence of stabilizers. SLS exhibited endothermic melting peaks at 114.9 °C and 181.7 °C. However, the endothermic melting peaks of SLS were not observed in CLD-NS, which may indicate that SLS was transformed into an amorphous state during the milling-drying process [34]. CLD-NS showed significantly different DSC thermograms compared with bulk CLD and CLD-PM, as the melting point peak of CLD-NS decreased to 102.1 °C and the peak intensity became very weak. This change in peak position and melting temperature may have been due to the formation of crystal defects and crystal lattice disorders during the milling-drying process [35–37], which demonstrated that some of the crystalline CLD was transformed into an amorphous state. In addition, this phenomenon was probably due to the miscibility of the drug with excipients and particle size reduction [9,38].

3.3. PXRD

To test the obtained DSC results and further confirm the crystalline state of various samples, PXRD analysis was conducted and the X-ray diffractograms are shown in Fig. 3. For bulk CLD, characteristic sharp peaks were seen at 2θ of 5.90°, 11.78°, 14.36°, 16.58°, 18.67°, 21.83°, and 29.61°. In addition, the characteristic diffraction peaks of bulk CLD were also obtained with the physical mixtures, suggesting that the mixing process did not affect the crystalline structure of CLD. However, in the case of CLD-NS, the position of most distinct crystalline peaks remained unchanged compared to bulk CLD and CLD-PM, but with lower peak intensity and relatively rough amorphous patterns, which may have been due to the reduced particle size after milling [11] and coverage of CLD by the excipients [37]. These PXRD results were consistent with those obtained in the aforementioned DSC experiment. When combining the results of DSC and PXRD, it was clearly seen that the crystalline structure was retained after milling-drying despite the fact that some of the crystalline CLD was transformed into an amorphous state to form a coexisting system.

3.4. FT-IR

FT-IR spectroscopy was also used to investigate the possibility of molecular interactions between the drug and stabilizers. The FT-IR spectra of CLD coarse powder, PVP VA64, SLS, physical mixtures and CLD-NS are shown in Fig. 4. The CLD coarse powder exhibited characteristic FTIR absorption peaks at 3292 cm^{-1} (N–H stretching vibration), 1697 cm^{-1} (C=O stretching), 1649 cm^{-1} and 1623 cm^{-1} (C=C stretching), 1524 cm^{-1} and 1348 cm^{-1} (NO_2 stretching) and 1137 cm^{-1} and 1623 cm^{-1} (-O-CH3 deformation vibration and stretching). All characteristic CLD peaks were detected in physical mixtures and CLD-NS. Furthermore, there was no obvious shift in wave number and other significant disappearances in the spectrum and most of the CLD peaks were maintained, demonstrating that there were no detectable interactions between the functional groups of CLD and stabilizers as well as good compatibility between drugs and excipients.

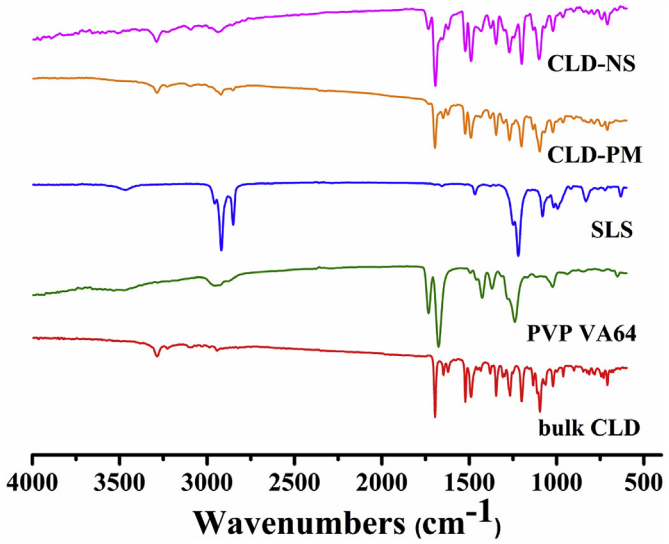

Fig. 4. FT-IR spectra of CLD powder, PVP VA64, SLS, physical mixtures of CLD, PVP VA64 and SLS and CLD-NS powder.

3.5. Raman spectroscopy

The Raman spectra of CLD coarse powder, PVP VA64, SLS, physical mixtures and CLD-NS between 3200 and 200 cm^{-1} are shown in Fig. 5. The strong bonds in Raman spectra of both CLD coarse powder and physical mixtures at 997 cm^{-1} and 1345 cm^{-1}, corresponded with Raman-active aromatic ring breathing and C–N stretching modes [39]. In addition, the Raman peaks of the stretching vibration of C=C ($\nu_{C=C}$, 1640 cm^{-1}), stretching vibration of C–H aliphatic (ν_{C-H}, 2942 cm^{-1}, 3061 cm^{-1}) and carbonyl ($\nu_{C=O}$, 1696 cm^{-1}) moieties in the ester group were observed in the spectra of CLD coarse powder and physical mixtures. By contrast, in the case of CLD-NS, all characteristic Raman peaks moved to high wave numbers, such as aromatic ring breathing (1080 cm^{-1}), C–N stretching modes (1394 cm^{-1}), C=C stretch (1660 cm^{-1}) and C–H aliphatic stretch (3042 cm^{-1}, 3087 cm^{-1}). In addition, the peak intensity became very weak compared with the CLD coarse powder and physical mixtures. This was possibly due to crystal disorder, lattice strain (induced by the surrounding medium) or surface relaxation (induced by a solid/solid interface), which can cause changes in Raman bands [40]. These results suggested that the formation of crystal defects and partial amorphous drug during the wet-milling process, which were also supported by the DSC and PXRD results.

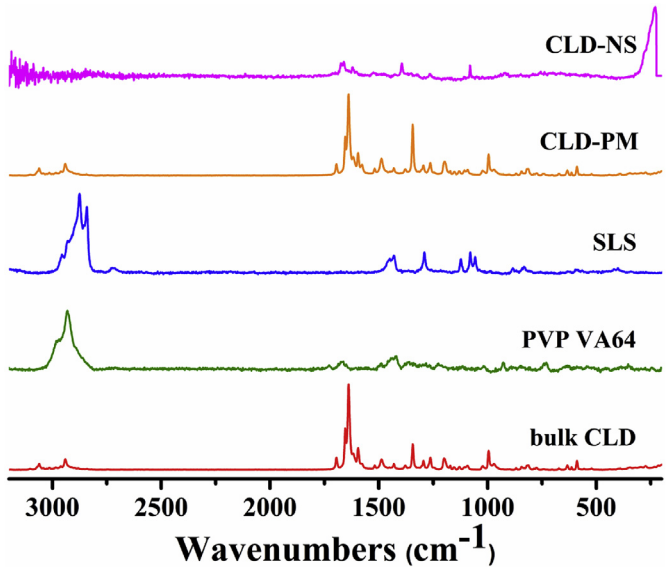

Fig. 5. Raman spectra of CLD powder, PVP VA64, SLS, physical mixtures of CLD, PVP VA64 and SLS and CLD-NS powder.

3.6. Stability of CLD nanosuspensions

The physical stability of prepared CLD-NS was determined under refrigerated conditions (4 °C) and at room temperature for 4 weeks. The results are detailed in Table 1. Particle size, PDI, and zeta potential after 4 weeks in the different storage conditions were not significantly different to fresh CLD-NS, suggesting that the prepared CLD-NS was stable for 4 weeks at 4 °C and room temperature. However, the change in particle size and PDI of CLD-NS stored at room temperature was irregular, while at 4 °C a continuous slight increase in particle size and PDI from the first day to 4 weeks was observed. The zeta potential of CLD-NS was almost unchanged in both conditions. These results indicated that the fabricated CLD-NS was physically stable.

The excellent stability of CLD-NS could be due to the synergism between PVP VA64 and SLS, which were selected as the polymer carrier and anionic stabilizer, respectively. PVP VA64 with a long chain is adsorbed onto the surface of CLD, thereby limiting CLD particle movement and provided steric stabilization for CLD-NS. Furthermore, the negative charges (approximately −30 mV) on the surface of CLD nanoparticles, which originated from adsorbed SLS, provided electrostatic repulsion by forming an electrical double layer, which prevented the aggregation of CLD particles. In addition, the presence of SLS may facilitate PVP VA64 adsorption to form a co-adsorbed layer, which resulted in electrostatic stabilization of CLD-NS [30,41,42].

3.7. Saturation solubility and in vitro dissolution

The saturation solubilities of bulk CLD, physical mixtures, and lyophilized CLD-NS powder were 0.30 ± 0.24, 3.28 ± 0.18, and 16.36 ± 1.36 μg/mL, respectively. The saturation solubility of CLD-NS markedly improved solubility compared with bulk CLD and CLD-PM, which was mainly attributed to the reduced particle size of CLD-NS and the solubilization effect of PVP VA64 and SLS.

The dissolution profiles of bulk CLD, physical mixtures and CLD-NS powder in different dissolution media are shown in Fig. 6. Bulk CLD powder exhibited dissimilar dissolution behavior in pH 1.2 hydrochloric acid solution, distilled water and pH 6.8 phosphate buffer. The dissolution of bulk CLD powder was only 7.13% (Fig. 6a) at 60 min in pH 1.2 hydrochloric acid solution and 24.92% (Figs. 6b) and 24.30% (Fig. 6c) in distilled water and pH 6.8 phosphate buffer, respectively. These findings demonstrated that CLD powder was more difficult to dissolve in pH 1.2 hydrochloric acid solution. The physical mixtures displayed similar dissolution properties over 60 min in the three dissolution media and showed a slight increase at different time points compared with bulk CLD powder, but the accumulated dissolution was just 30% at 60 min. This could be due to the presence of excipients, which enhanced particle wettability and improved dissolution. With regard to the CLD-NS powder, markedly enhanced dissolution velocities were observed in all media. More than 70% of the drug in the nanosuspension was released within 5 min and approximately 90% was released at 60 min. The similarity factor f_2 for the dissolution profiles between CLD-NS powder and bulk CLD powder was only 5.41, 5.35 and 3.17 in the above three dissolution media, respectively, and the f_2 was also less than 8 between CLD-NS and the physical mixtures. These results demonstrated that dissolution of CLD-NS was distinctly superior compared to bulk CLD powder and physical mixtures. Consequently, it was concluded that the improvement in dissolution rate of CLD-NS was mainly attributable to the reduction in particle size to the nanometer range and the increased surface area of CLD nanoparticles. Moreover, PVP VA64 markedly enhanced drug particle wettability and solubility. Similar experimental results were reported in previous research [26,43]. Additionally, the presence of partial amorphous CLD also

Table 1
Stability index of CLD nanosuspensions (mean ± SD, n = 3).

Formula	Time (week)	At refrigerated temperature (4 °C)			At room temperature		
		Size (nm)	PDI	ZP (mV)	Size (nm)	PDI	ZP (mV)
CLD-NS	0	312.15 ± 7.19	0.11 ± 0.01	−33.63 ± 0.87	312.15 ± 7.19	0.11 ± 0.01	−33.63 ± 0.87
	2	318.87 ± 5.11	0.11 ± 0.02	−33.37 ± 0.68	346.54 ± 4.85	0.24 ± 0.01	−32.80 ± 0.37
	4	320.40 ± 7.88	0.18 ± 0.05	−34.53 ± 0.62	331.26 ± 3.47	0.30 ± 0.02	−30.53 ± 1.21

played a key role in promoting dissolution, as an amorphous drug with high internal energy and molecular motion is beneficial in increasing the dissolution rate [20,44,45].

3.8. *In vivo* pharmacokinetics

The *in vivo* pharmacokinetics of CLD powder, CLD capsule and CLD-NS powder were investigated and compared in SD rats. The CLD plasma concentration-time profiles were plotted and are shown in Fig. 7, and the main pharmacokinetic parameters are summarized in Table 2. As shown, the maximum drug concentration in plasma (C_{max}) and the area under the curve (AUC_{0-24}) of CLD-NS were approximately 3.13-fold and 2.38-fold higher than those of bulk CLD, respectively. Moreover, the C_{max} and AUC_{0-24} of CLD-NS increased by approximately 1.65-fold and 2.17-fold, compared with the commercial capsule. In addition, T_{max} of the commercial capsule and CLD-NS was shorter than the CLD-suspension. The relative bioavailability of CLD-NS was 238.27% and 216.67% in comparison to the CLD coarse suspension and commercial capsule, respectively. These findings were consistent with the *in vitro* dissolution results. Thus, the observed pharmacokinetic results strongly demonstrated that the oral bioavailability of CLD in rats was markedly enhanced by the CLD nanosuspension formulation.

To our knowledge, in the past few decades, no studies have used pharmaceutical techniques to improve the bioavailability of CLD, with the exception of studies which focused on the pharmacokinetic methodology of CLD [46,47]. In this study, the improved oral bioavailability of CLD-NS was probably due to several factors. First, due to the reduced particle size of CLD-NS and solubilization of PVP VA64 [26,44], the solubility and *in vitro* dissolution rate significantly increased, which improved oral bioavailability. Second, when CLD-NS enters the gastrointestinal tract, nanoparticles can greatly improve membrane permeation by increasing the adhesion surface area between nanoparticles and intestinal epithelium membranes [12] or cross the intestinal membranes and enter the blood circulation [42,48]. These potential mechanisms of CLD-NS absorption through the gastrointestinal tract should be confirmed in future studies.

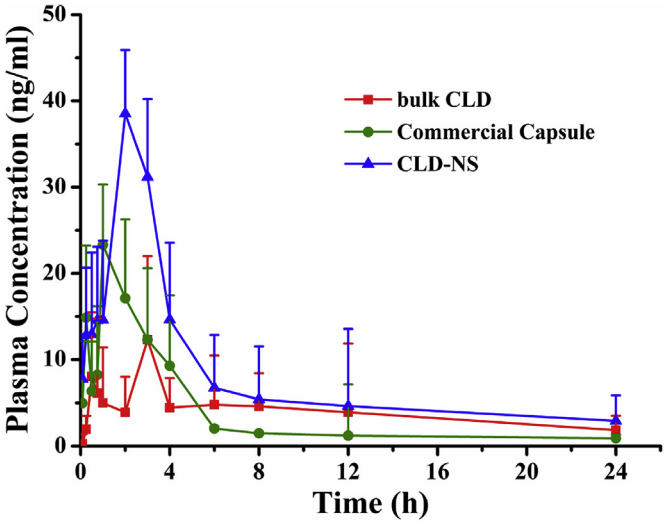

Fig. 7. CLD Plasma concentration-time curves in rats after oral administration of bulk CLD, Commercial Capsule and CLD-NS (mean ± SD, n = 6).

Table 2
Pharmacokinetic parameters after single oral administration of CLD formulations to rats at a dose of 2 mg/kg (mean ± SD, n = 6).

Parameters	CLD suspension	Commercial Capsule	CLD-NS
C_{max} (ng/ml)	12.30 ± 2.17	23.30 ± 7.01[d]	38.52 ± 7.38[a,c]
t_{max} (h)	3 ± 1.30	1 ± 0.14	2 ± 1.80
$t_{1/2}$ (h)	3.39 ± 3.74	2.07 ± 2.56	2.37 ± 0.65
AUC_{0-24h} (ng h/ml)	80.88 ± 23.67	88.94 ± 41.57[d]	192.71 ± 46.75[a,c]
$AUC_{0-\infty}$ (ng h/ml)	102.05 ± 18.15	119.19 ± 40.60[d]	235.67 ± 16.66[b,c]

[a] $p < 0.05$ and.
[b] $p < 0.01$ when CLD-NS was compared with CLD-suspension.
[c] $p < 0.05$ when CLD-NS was compared with Commercial Capsule.
[d] $p < 0.05$ when Commercial Capsule was compared with CLD-suspension.

4. Conclusions

In this study, CLD-NS was successfully prepared by the wet-milling method using PVP VA64 and SLS as stabilizers. The average particle size, PDI, and zeta potential of the prepared CLD-NS were 312.15 ± 7.19 nm, 0.11 ± 0.01, and −33.63 ± 0.87 mV, respectively. Furthermore, physicochemical characterization of CLD-NS illustrated that a portion of crystalline CLD was transformed into an amorphous state during the milling-drying process and was physically stable for 4 weeks in different temperature conditions. In addition, the

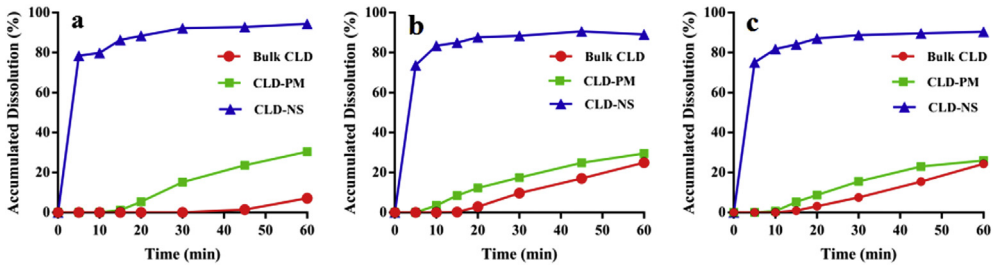

Fig. 6. Dissolution profiles for bulk CLD powder, physical mixtures powder and CLD-NSs in different dissolution media with 0.1% tween-80 (a pH 1.2 hydrochloric acid solution; b distilled water; c pH 6.8 phosphate buffer)(mean ± SD, n = 6).

in vitro dissolution of CLD-NS was markedly enhanced compared with bulk CLD and CLD-PM. The subsequent *in vivo* pharmacokinetic study indicated significantly improved oral bioavailability of CLD-NS in rats. In conclusion, the CLD-NS established in this study could be a suitable strategy for enhancing the dissolution and oral bioavailability of CLD.

Declaration of competing interest

The authors declare no potential conflict of interest. The authors alone are responsible for the design of the study, the content and writing of the manuscript.

Acknowledgements

We thank the Science and Technology Program of Ningxia Province (NXZY201713) for financially supporting this work.

References

[1] H. Tandel, M. Upadhay, K. Raval, A. Nayani, Preparation and evaluation of cilnidipine microemulsion, J. Pharm. BioAllied Sci. 4 (2012) 114–115.
[2] S. Saboo, N.A. Mugheirbi, D.Y. Zemlyanov, U.S. Kestur, L.S. Taylor, Congruent release of drug and polymer: a “sweet spot” in the dissolution of amorphous solid dispersions, J. Control. Release 298 (2019) 68–82.
[3] A.S. Indulkar, G. Yi, S.A. Raina, G.G.Z. Zhang, L.S. Taylor, Crystallization from supersaturated solutions: role of lecithin and composite simulated intestinal fluid, Pharm. Res. 35 (2018) 158–171.
[4] Y. Chen, C. Liu, Z. Chen, C. Su, M. Hageman, R. Haskell, K. Stefanski, F. Qian, Drug-polymer-water interaction and its implication for the dissolution performance of amorphous solid dispersions, Mol. Pharm. 12 (2015) 576–589.
[5] C. Chen, X. Xie, Y. Li, C. Zhou, Y. Song, Z. Yan, X. Yang, Influence of different polymers on crystallization tendency and dissolution behavior of cilnidipine in solid dispersions, Drug Dev. Ind. Pharm. 40 (2014) 441–451.
[6] L. Hu, H. Zhang, W. Song, D. Gu, Q. Hu, Investigation of inclusion complex of cilnidipine with hydroxypropyl-β-cyclodextrin, Carbohydr. Polym. 90 (2012) 1719–1724.
[7] S.S. Bakhle, J.G. Avari, Development and characterization of solid Self-emulsifying drug delivery system of cilnidipine, Chem. Pharmaceut. Bull. 63 (2015) 408–417.
[8] S.K. Nagar, M.M. Soniwala, Optimization of cilnidipine nanosuspension using a center composite design, Int. J. Pharm. Sci. Drug Res. 9 (2017) 149–159.
[9] Y. Wang, C. Wang, J. Zhao, Y. Ding, L. Li, A cost-effective method to prepare curcumin nanosuspensions with enhanced oral bioavailability, J. Colloid Interface Sci. 485 (2017) 91–98.
[10] J. He, Y. Han, G. Xu, L. Yin, M.N. Neubi, J. Zhou, Y. Ding, Preparation and evaluation of celecoxib nanosuspensions for bioavailability enhancement, RSC Adv. 7 (2017) 13053–13064.
[11] S. Huang, Q. Zhang, H. Li, Y. Sun, G. Cheng, M. Zou, H. Piao, Increased bioavailability of efonidipine hydrochloride nanosuspensions by the wet-milling method, Eur. J. Pharm. Biopharm. 130 (2018) 108–114.
[12] Q. Fu, B. Li, D. Zhang, M. Fang, J. Shao, M. Guo, Z. Guo, M. Li, J. Sun, J. Zhai, Comparative studies of the in vitro dissolution and in vivo pharmacokinetics for different formulation strategies (solid dispersion, micronization, and nanocrystals) for poorly water-soluble drugs: a case study for lacidipine, Colloids Surfaces B Biointerfaces 132 (2015) 171–176.
[13] R.H. Muller, S. Gohla, C.M. Keck, State of the art of nanocrystals-Special features, production, nanotoxicology aspects and intracellular delivery, Eur. J. Pharm. Biopharm. 78 (2011) 1–9.
[14] Y. Zhou, Q. Fang, B. Niu, B. Wu, Y. Zhao, G. Quan, X. Pan, C. Wu, Comparative studies on amphotericin B nanosuspensions prepared by a high pressure homogenization method and an antisolvent precipitation method, Colloids Surfaces B Biointerfaces 172 (2018) 372–379.
[15] Djordje Medarević, Jelena Djuriš, Svetlana Ibrić, Miodrag Mitrić, K. Kachrimanis, Optimization of formulation and process parameters for the production of carvedilol nanosuspension by wet media milling, Int. J. Pharm. 540 (2018) 150–161.
[16] Yosuke Kuroiwa, Kenjirou Higashi, Keisuke Ueda, K. Yamamoto, K. Moribe, Nanoscale and molecular-level understanding of wet-milled indomethacin/poloxamer 407 nanosuspension with TEM, suspended-state NMR, and Raman measurements, Int. J. Pharm. 537 (2018) 30–39.
[17] Y. Li, Z. Wu, W. He, C. Qin, J. Yao, J. Zhou, L. Yin, Globular protein-coated Paclitaxel nanosuspensions: interaction mechanism, direct cytosolic delivery, and significant improvement in pharmacokinetics, Mol. Pharm. 12 (2015) 1485–1500.
[18] Y. Wang, Y. Zheng, L. Zhang, Q. Wang, D. Zhang, Stability of nanosuspensions in drug delivery, J. Control. Release 172 (2013) 1126–1141.
[19] E.M. Merisko-Liversidge, G.G. Liversidge, Drug nanoparticles: formulating poorly water-soluble compounds, Toxicol. Pathol. 36 (2008) 43–48.
[20] L. Wu, J. Zhang, W. Watanabe, Physical and chemical stability of drug nanoparticles, Adv. Drug Deliv. Rev. 63 (2011) 456–469.
[21] A. Bhakay, M. Rahman, R. Dave, E. Bilgili, Bioavailability enhancement of poorly water-soluble drugs via nanocomposites: formulation-processing aspects and challenges, Pharmaceutics 10 (2018) 1–62.
[22] A. Tuomela, J. Hirvonen, L. Peltonen, Stabilizing agents for drug nanocrystals: effect on bioavailability, Pharmaceutics 8 (2016) 1–16.
[23] S. Verma, B.D. Huey, D.J. Burgess, Scanning probe microscopy method for nanosuspension stabilizer selection, Langmuir 25 (2009) 12481–12487.
[24] E.M. Merisko-Liversidge, G.G. Liversidge, Nanosizing for oral and parenteral drug delivery: a perspective on formulating poorly-water soluble compounds using wet media milling technology, Adv. Drug Deliv. Rev. 63 (2011) 427–440.
[25] M. Li, M. Azad, R. Davé, E. Bilgili, Nanomilling of drugs for bioavailability enhancement: a holistic formulation-process perspective, Pharmaceutics 8 (2016) 17–51.
[26] C. Zhu, S. Gong, J. Ding, M. Yu, E. Ahmad, Y. Feng, Y. Gan, Supersaturated polymeric micelles for oral silybin delivery: the role of the Soluplus-PVPVA complex, Acta Pharm. Sin. B 9 (2018) 107–117.
[27] S.R. Shah, R.H. Parikh, J.R. Chavda, N.R. Sheth, Glibenclamide nanocrystals for bioavailability enhancement: formulation design, process optimization, and pharmacodynamic evaluation, J. Pharm. Innov. 9 (2014) 227–237.
[28] K. Hye-In, P. Sang, P. Seok, L. Jewon, C. Kwan, J. Jun-Pil, K. Hee-Che, M. Han-Joo, J. Dong-Jin, Development and evaluation of a reconstitutable dry suspension to improve the dissolution and oral absorption of poorly water-soluble celecoxib, Pharmaceutics 10 (2018) 140–154.
[29] H. Yang, H. Kim, S. Jung, H. Seo, S.K. Nida, S.Y. Yoo, J. Lee, Pharmaceutical strategies for stabilizing drug nanocrystals, Curr. Pharmaceut. Des. 24 (2018) 2362–2374.
[30] M. Li, P. Alvarez, P. Orbe, E. Bilgili, Multi-faceted characterization of wet-milled griseofulvin nanosuspensions for elucidation of aggregation state and stabilization mechanisms, AAPS PharmSciTech 19 (2018) 1789–1801.
[31] L. Zong, X. Li, H. Wang, Y. Cao, L. Yin, M. Li, Z. Wei, D. Chen, X. Pu, J. Han, Formulation and characterization of biocompatible and stable I.V. itraconazole nanosuspensions stabilized by a new stabilizer polyethylene glycol-poly(β-Benzyl-L-aspartate) (PEG-PBLA), Int. J. Pharm. 531 (2017) 108–117.
[32] Y. Zhou, J. Du, L. Wang, Y. Wang, Nanocrystals technology for improving bioavailability of poorly soluble drugs: a mini-review, J. Nanosci. Nanotechnol. 17 (2017) 18–28.
[33] M. Li, L. Zhang, R. Davé, E. Bilgili, An intensified vibratory milling process for enhancing the breakage kinetics during the preparation of drug nanosuspensions, AAPS PharmSciTech 17 (2016) 389–399.
[34] D. Liu, H. Xu, B. Tian, K. Yuan, H. Pan, S. Ma, X. Yang, W. Pan, Fabrication of carvedilol nanosuspensions through the anti-solvent precipitation-ultrasonication method for the improvement of dissolution rate and oral bioavailability, AAPS PharmSciTech 13 (2012) 295–304.
[35] D.F. Odetade, G.T. Vladisavljevic, Microfluidic fabrication of hydrocortisone nanocrystals coated with polymeric stabilisers, Micromachines 7 (2016) 1–17.
[36] H. Yang, F. Teng, P. Wang, B. Tian, X. Lin, X. Hu, L. Zhang, X. Zhang, Y. Zhang, X. Tang, Investigation of a nanosuspension stabilized by Soluplus® to improve bioavailability, Int. J. Pharm. 477 (2014) 88–95.
[37] E. Bilgili, M. Rahman, D. Palacios, F. Arevalo, Impact of polymers on the aggregation of wet-milled itraconazole particles and their dissolution from spray-dried nanocomposites, Adv. Powder Technol. (2016) 1–16.
[38] B.K. Ahuja, S.K. Jena, S.K. Paidi, S. Bagri, S. Suresh, Formulation, optimization and in vitro–in vivo evaluation of febuxostat nanosuspension, Int. J. Pharm. 478 (2015) 540–552.
[39] D. Li, M. Wang, C. Yang, J. Wang, G. Ren, Solid state characterizations and analysis of stability in azelnidipine polymorphs, Chem. Pharm. Bull. 60 (2012) 995–1002.
[40] Y. Chen, L. Ma, Y. Yin, X. Qian, G. Zhou, X. Gu, F. Zhang, Strong quantum confinement effect in Cu_4SnS_4, quantum dots synthesized via an improved hydrothermal approach, J. Alloy. Comp. 672 (2016) 204–211.
[41] E. Bilgili, M. Li, A. Afolabi, Is the combination of cellulosic polymers and anionic surfactants a good strategy for ensuring physical stability of BCS Class II drug nanosuspensions? Pharm. Dev. Technol. 21 (2016) 499–510.
[42] A.M. Cerdeira, M. Mazzotti, B. Gander, Miconazole nanosuspensions: influence of formulation variables on particle size reduction and physical stability, Int. J. Pharm. 396 (2010) 210–218.
[43] Y. Zhao, X. Xie, Y. Zhao, Y. Gao, C. Cai, Q. Zhang, Z. Ding, Z. Fan, H. Zhang, M. Liu, J. Han, Effect of plasticizers on manufacturing ritonavir/copovidone solid dispersions via hot-melt extrusion: preformulation, physicochemical characterization, and pharmacokinetics in rats, Eur. J. Pharm. Sci. 127 (2018) 60–70.
[44] Prachi Shekhawat, Varsha Pokharkar, Risk assessment and QbD based optimization of an Eprosartan mesylate nanosuspension: in-vitro characterization, PAMPA and in-vivo assessment, Int. J. Pharm. 567 (2019) 1–18.
[45] H. Qiao, L. Chen, T. Rui, J. Wang, T. Chen, T. Fu, J. Li, L. Di, Fabrication and in vitro/in vivo evaluation of amorphous andrographolide nanosuspensions stabilized by D-α-tocopheryl polyethylene glycol 1000 succinate/sodium lauryl sulfate, Int. J. Nanomed. 12 (2017) 1033–1046.
[46] L. Heonwoo, S. Jihyung, L. Hyunsu, J. Seoyoung, C. Youngwuk, L. Kyungtae, Development of a liquid chromatography/negative-ion electrospray tandem mass spectrometry assay for the determination of cilnidipine in human plasma and its application to a bioequivalence study, J. Chromatogr. B 862 (2008) 246–251.
[47] X. Zhang, S. Zhai, R. Zhao, J. Ouyang, X. Li, W.R. Baeyens, Determination of cilnidipine, a new calcium antagonist, in human plasma using high performance liquid chromatography with tandem mass spectrometric detection, Anal. Chim. Acta 600 (2007) 142–146.
[48] F. Xia, W.F. Fan, S.F. Jiang, Y. Ma, Y. Lu, J. Qi, E. Ahmad, X. Dong, W. Zhao, W. Wu, Size-dependent translocation of nanoemulsions via oral delivery, ACS Appl. Mater. Interfaces 9 (2017) 21660–21672.